SCIENCE CHINA
Physics, Mechanics & Astronomy

• Article •

November 2012 Vol.55 No.11: 2186–2193
doi: 10.1007/s11433-012-4897-0

Estimation of the inter-frequency clock bias for the satellites of PRN25 and PRN01

LI HaoJun[1,2*], ZHOU XuHua[1], WU Bin[1,2] & WANG JieXian[3]

[1] *Shanghai Astronomical Observatory, Chinese Academy of Sciences, Shanghai 200030, China;*
[2] *Shanghai Key Laboratory of Space Navigation and Position Techniques, Shanghai 200030, China;*
[3] *Department of Surveying and Geo-informatics Engineering, Tongji University, Shanghai 200092, China*

Received April 11, 2012; accepted May 18, 2012; published online September 17, 2012

We present two efficient approaches, namely the epoch-differenced (ED) and satellite- and epoch-differenced (SDED) approaches, for the estimation of IFCBs of the two Block IIF satellites. For the analysis, data from 18 stations from the IGS network spanning 96 d is processed. Results show that the IFCBs of PRN25 and PRN01 exhibit periodical signal of one orbit revolution with a magnitude up to 18 cm. The periodical variation of the IFCBs is modeled by a sinusoidal function of the included angle between the sun, earth and the satellite. The presented model enables a consistent use of L1/L2 clock products in L1/L5-based positioning. The algorithm is incorporated into the MGPSS software at SHAO (Shanghai Astronomical Observatory, Chinese Academy of Sciences) and is used to monitor the IFCB variation in near real-time.

triple-frequency signals, precise point positioning, inter-frequency clock bias

PACS number(s): 06.30.Gv, 91.10.By, 91.10.Fc, 93.85.Bc

Citation: Li H J, Zhou X H, Wu B, et al. Estimation of the inter-frequency clock bias for the satellites of PRN25 and PRN01. Sci China-Phys Mech Astron, 2012, 55: 2186–2193, doi: 10.1007/s11433-012-4897-0

1 Introduction

The development of Global Navigation Satellite Systems (GNSS), including the US modernized Global Positioning System (GPS), the European Galileo system, the Japanese Quasi-Zenith Satellite System (QZSS) and Chinese COMPASS system provide observations in more frequencies, which may benefit the GNSS technology and applications [1,2]. The application of triple-frequency combinations has been demonstrated in ambiguity resolution [3–5], relative precise positioning as well as ionospheric tomography [6,7].

The latest generational version of GPS satellite, Block IIF, provides additional L5 signal, which enhances the aeronautical safety-of-life applications. An enhanced rubidium frequency standard was provided by PerkinElmer, and the Xenon lamp buffer gas and a thin-film spectral filter in the physics package are used to reduce shot noise and improve the signal-to-noise ratio [8]. The current in-orbit Block IIF satellites are SVN62/PRN25 and SVN63/PRN01 that were launched in May 2010 and July 2011, respectively. An apparent inconsistency between three frequency carrier phases of PRN25 was noted by the scientific community, which was understood to be caused by thermally dependent inter-frequency bias (IFB) [8,9], which differs in each satellite. In the current clock estimations, L1/L2 based ionosphere-free linear combination is normally used, and the impacts of IFBs exist in satellite clocks. Consequently, the satellite clocks derived from L1/L2 carrier-phase observations cannot be used for L1/L5 based PPP positioning without careful consideration of these biases. In the relative positioning, the IFBs could be completely negated as a common error by making differences between receivers. However, the IFB

*Corresponding author (email: yanlhjch@126.com)

contaminates the precise point positioning (PPP) [10] solutions as these biases may partly go into undifferenced ambiguities.

Montenbruck et al. [8] showed that the L1/L2 clock offsets exhibited 1/rev and 2/rev dominated periodical variations with an amplitude up to 15 cm. They also estimated the inter-frequency clock biases (IFCBs) of PRN25 based on the difference of the two ionosphere-free phase combinations (L1/L5-minus-L1/L2). Their results showed that the IFCBs show complex periodical signals with amplitude up to 20 cm. In their IFCBs estimation, they neglected the contribution of the receiver.

For the estimation of IFCBs, undifferenced phase observations of a global network are normally used, which involves the estimation of large number of ambiguities and epoch-wise bias parameters. To improve the computation efficiency, two efficient approaches were taken, namely epoch-differenced (ED) [11] and satellite- and epoch-differenced (SDED) [12,13] in the estimation of IFCB. The presented approaches remove the ambiguity parameters and only ED or SDED IFCBs remain. Selecting a reference epoch and setting a referenced IFCB, the reference epoch based IFCB is then computed by using the estimated ED or SDED IFCB. To study the features of the IFCBs and evaluate the presented approaches, data from 18 stations from the IGS network spanning 96 d (DOY 224 to DOY 319, 2011) is processed. The periodical variations of the IFCBs of PRN25 and PRN01 are discussed in detail and a model is developed for the prediction of IFCB. In this paper, sect. 2 introduces the triple-frequency ionosphere-free measurements. Sect. 3 introduces the strategies for IFCB estimation. Sect. 4 presents the data analysis and discusses the results and finally. Sect. 5 summarizes the main findings.

2 Triple-frequency ionosphere-free measurements

The triple-frequency phase $L_r^s(k)$ (k=1, 2, 5) observation equations between satellite s and station r read as:

$$\begin{aligned} L_r^s(k) &= \rho + T + (dt_r + b_r) - (dt^s + b^s) \\ &\quad - I_1 \cdot f_1^2 / f_k^2 + const \\ &= \rho + T + \overline{dt}_r - \overline{dt}^s \\ &\quad - I_1 \cdot f_1^2 / f_k^2 + const, \end{aligned} \tag{1}$$

where ρ is the satellite-to-receiver range, T is the tropospheric delay, dt_r is the receiver clock and has been grouped with station-specific bias b_r and dt^s denotes the satellite clock offset term and has been grouped with a satellite-specific bias b^s. Both clock terms in the observation equation are considered to be signal and time dependent, denoted as $\overline{dt}_r$ and $\overline{dt}^s$. The I_1 is the ionospheric delay of L1, while *const* reflects a signal- and pass-specific carrier phase ambiguity.

The ionosphere-free measurements between frequencies i and j can be defined as:

$$\begin{aligned} IF(L_j, L_i) &= \frac{f_j^2}{f_j^2 - f_i^2} \cdot L_j - \frac{f_i^2}{f_j^2 - f_i^2} \cdot L_i \\ &= \rho + T + \overline{dt}_r(i,j) - \overline{dt}^s(i,j) + const_{if} \\ &= \rho + T + \delta_{i,j} + const_{if}, \end{aligned} \tag{2}$$

where $\overline{dt}_r(i,j)$ and $\overline{dt}^s(i,j)$ are station and satellite phase clocks of the ionosphere-free measurements between frequency i and j and have been grouped into term $\delta_{i,j}$, $const_{if}$ is the ionosphere-free carrier phase ambiguity. The geometric range and tropospheric delay can be removed by differencing two different ionosphere-free measurements (L1/L2 and L1/L5), and the remaining terms are ambiguity and IFCBs. The differenced ionosphere-free measurement (DIF) can be written as:

$$\begin{aligned} DIF(L_1, L_2, L_5) &= IF(L_1, L_2) - IF(L_1, L_5) \\ &= (\delta_{1,2} - \delta_{1,5}) + const_3 - const_6, \end{aligned} \tag{3}$$

where $const_3$ is the ambiguity of ionosphere-free combination formed with L_1 and L_2, $const_6$ is the ambiguity of ionosphere-free combination formed with L_1 and L_5, and the term $\delta_{1,2}-\delta_{1,5}$ is the IFCB between phase clock of the L1/L2 and L1/L5 combinations. Based on eq. (3), the IFCB can be estimated in a general clock estimation procedure [8]. However, such strategy is time consuming and complex handling of ambiguities is needed.

3 Fast estimation of IFCB

Eq. (3) indicates that not only the satellite but also the station which contributes to the total DIF value. To study the property of the IFCB of satellites through the DIF observations, the contribution of the receiver has to be removed. Two strategies derived from the ED and SDED DIF phase measurements are introduced in the determination of satellite IFCB in this section.

3.1 ED IFCB

From eq. (3) we have

$$\begin{aligned} \delta &= \delta_{1,2} - \delta_{1,5} \\ &= DIF(L_1, L_2, L_5) - const_3 + const_6. \end{aligned} \tag{4}$$

Assuming there is no cycle slip between two adjacent epochs, the ambiguity term in eq. (3) can be eliminated by differencing the DIF phase measurement at epoch m and

m–1. We can obtain

$$\Delta\delta(m) = (\delta_{1,2} - \delta_{1,5})(m) = DIF(L_1, L_2, L_5)(m) - DIF(L_1, L_2, L_5)(m-1), \quad (5)$$

where "Δ" indicates the ED operator; $\Delta\delta$ is the ED IFCB. Assuming there are n stations in the network, which improves the redundancy of the solution, the ED IFCB $\Delta\delta(m)$ can be calculated by averaging $\Delta\delta(m)_k$ over the entire network:

$$\Delta\delta(m) = \frac{1}{n} \cdot \sum_{k=1}^{n} \Delta\delta(m)_k. \quad (6)$$

Using the estimated ED IFCBs and the IFCB at the selected reference epoch, the reference epoch based IFCB at epoch m can be expressed as:

$$\delta(m) = \delta(m_0) + \sum_{n_1=1}^{np} \Delta\delta(n_1), \quad (7)$$

where $\delta(m_0)$ is the IFCB at the reference epoch m_0, $\Delta\delta(n_1)$ is the ED IFCB at epoch n_1, and np is the number of epochs between the reference epoch and epoch m.

3.2 SDED IFCB

The SDED IFCB can be derived directly by differing the ED IFCB between different satellites a and b.

$$\nabla\delta(m)^{a,b} = \Delta\delta(m)^b - \Delta\delta(m)^a. \quad (8)$$

In eq. (8), $\Delta\delta(m)^a$ and $\Delta\delta(m)^b$ are derived from eq. (6) based on the whole network. Because the groups of stations tracking satellite a and b are different at each epoch, the IFCB of the station still exists in eq. (8).

The method based on eq. (8) is referred to as "Approach 1" in the following sections. There is another approach termed "Approach 2" for SDED IFCB estimation. For one receiver tracking two satellites (a,b) simultaneously, the satellite-differenced DIF measurements can be used to eliminate the contribution of the receiver. By taking the differences of ED DIF phase measurements of satellites a and b, we obtain

$$\nabla\delta(m)^{a,b} = (\delta_{1,2} - \delta_{1,5})(m)^{a,b} = \Delta DIF(L_1, L_2, L_5)(m)^b - \Delta DIF(L_1, L_2, L_5)(m)^a. \quad (9)$$

The superscript "a,b" indicates the differences between satellite a and b, $\nabla\delta(m)^{a,b}$ is the SDED IFCB, which contains only satellite IFCB terms.

In "Approach 2", assuming there are n stations tracking two satellites (a,b) simultaneously, the SDED IFCB $\nabla\delta(m)^{a,b}$ can be calculated by averaging $\nabla\delta(m)^{a,b}{}_k$ over the network:

$$\nabla\delta(m)^{a,b} = \frac{1}{n} \cdot \sum_{k=1}^{n} \nabla\delta(m)_k^{a,b}. \quad (10)$$

From the definition of the two approaches, "Approach 1" is the difference based on mean ED IFCBs over the tracking network, therefore they contain the contribution of the stations. However, "Approach 2" eliminates the contribution of the station by making satellite difference at each station. Using the SDED IFCBs and the SD IFCB at the selected reference epoch, the SD IFCB can be computed by the following function:

$$\delta(m)^{a,b} = \delta(m_0)^{a,b} + \sum_{n_1=1}^{np} \nabla\delta(n_1)^{a,b}, \quad (11)$$

where $\delta(m_0)^{a,b}$ is the SD IFCB at the reference epoch m_0.

4 Data processing

To validate the presented approaches and study the performances of the IFCBs, the 96 d (DOY 224 to DOY 319, 2011) data from 18 stations from the IGS network is processed. Data is sampled at 30 s and the data of PRN01 is used from DOY 277 as the standard. Figure 1 shows the distribution of the 18 stations, which have the capability to track the new L5 signal of the Block IIF satellites.

4.1 ED IFCB

The ED IFCBs can be estimated by eq. (6). Figure 2 illustrates the epoch-wise ED IFCBs of the PRN25 and PRN01. From Figure 2, it can be observed that most of 30 s variations of the IFCB are at the sub-cm level, even though some variations reach up to ±20 mm. Figure 2 shows a typical result of clock differences between epochs, where the sum of residuals not equals to zero with short-term (epoch-wise) scatters representing clock jitter and observation noises. Daily mean ED IFCB in Figure 2, sampled at 30 s, is in the range of [–0.06, +0.06] mm, with which the daily IFCB may vary within [–18, +18] cm assuming the linear trend of ED IFCB. The estimated ED IFCBs could be used to evaluate the feasibility of the DIF phase measurement in cycle slip detection. Eq. (2) shows that although the DIF phase measurement removes geometric range and atmospheric delay, the measurement contains the receiver and satellite bias, which may vary over time. According to eq. (3), we calculate the change of DIF phase measurement by adding a slip of one cycle at L1, L2 and L5 frequency, respectively. Results show change of DIF phase is of 5.42, 37.75 and 32.13 cm respectively. Comparing these values to the variations of ED IFCBs, we see that the variation of ED IFCBs is much smaller than the DIF phase changes such as in the case of one cycle slip that occurred in one frequency. This

indicates that the IFCB variations will not affect the application of the DIF phase measurement in cycle slip detection when processing observations over the 30 s interval.

4.2 SD and SDED IFCBs between PRN01 and PRN25

SDED IFCBs are derived by implementing the two approaches as described in sect. 3. Figure 3 illustrates the SDED IFCBs between satellite PRN01 and PRN25, which vary at the range of ±0.07 m. Figure 4 shows the differences between the two approaches, from which we see that most differences are in the range of ±0.02 m. The mean of the differences is 0.01 mm.

Selecting GPS time 0:00 as reference epoch for each day, and set the initial SD IFCB $\delta(m_0)^{a,b}$ to 0, the SD IFCBs between PRN01 and PRN25 are estimated according to eq. (11). Figure 5 illustrates for DOY 307 the SD IFCBs based on different SDED IFCBs shown in Figure 3. These figures show that the results are based on two results have the same-peak values and trends. Comparing the two sets of results, Figure 6 shows the standard deviation of the differences, which gives a stable small value of less than 1 cm.

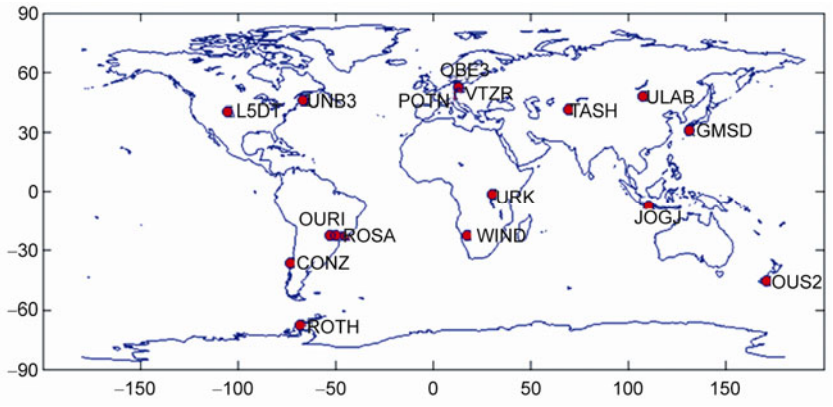

Figure 1 Distribution of the 18 stations tracking L5 signal.

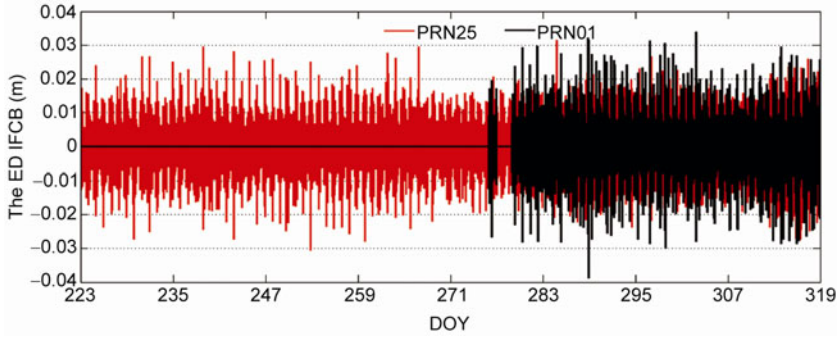

Figure 2 ED IFCB of PRN01 and PRN25.

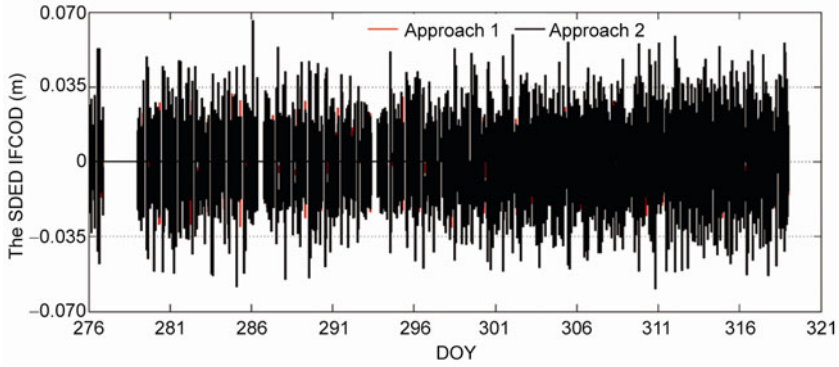

Figure 3 SDED IFCB of PRN01 and PRN25 under different approaches, where "Approach 1" refers to the SDED IFCBs based on eq. (8), while "Approach 2" denotes the results from eq. (10).

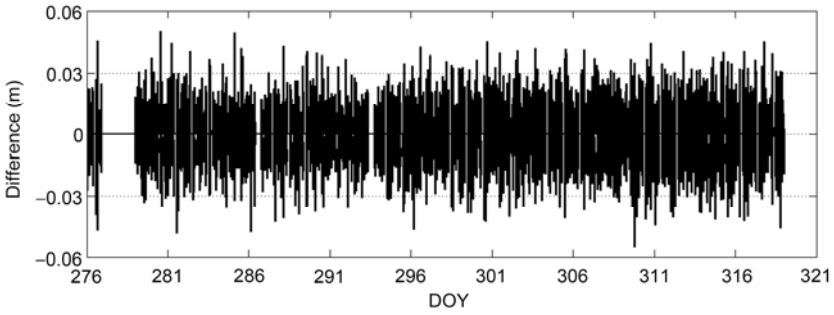

Figure 4 Difference between the two approaches of SDED IFCB.

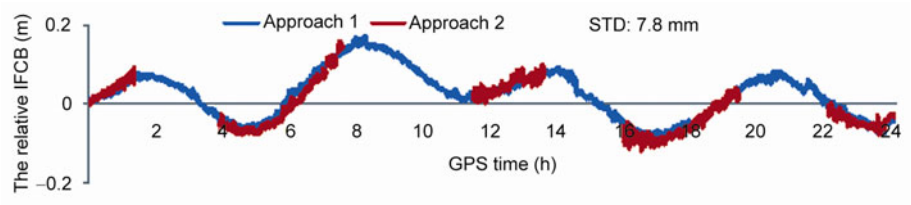

Figure 5 Two approaches for SD IFCB of DOY307.

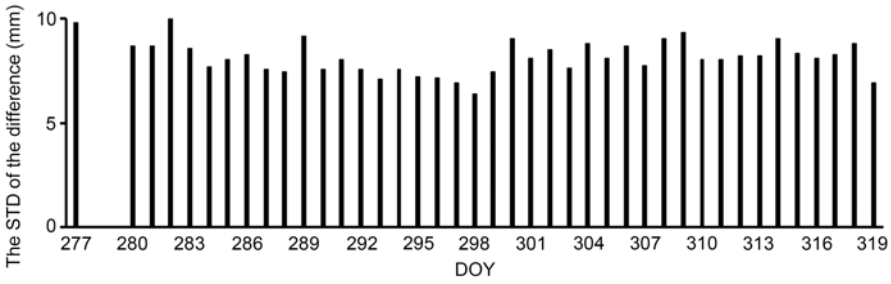

Figure 6 STD of the difference between the two approaches for SD IFCB.

The mean difference as stated previous is approximately 0.01 mm, therefore the STDs represent the jitters of IFCB and noise. Considering the small magnitude, the differences could be therefore ignored. The two approaches are thus generally equivalent. As the two approaches differs in the contribution of receiver IFCBs, our results validate the conclusion as stated by Montenbruck et al. [8] in that the contribution of the receiver can be neglected in IFCB estimation. Based on this conclusion, the station IFCBs will be ignored in the following sections.

4.3 Reference epoch based IFCB

Selecting GPS time 0:00 as reference epoch for each day, and set the initial IFCB $\delta(m_0)$ to 0, the IFCBs for PRN01 and PRN25 are estimated according to eq. (7). The 96 d reference epoch based IFCBs are given in Figure 7, which shows that the inter-frequency clock difference of the two satellites varies with time in the range of ±0.18 m.

Figure 8 shows the data for successive 3 d (DOY 307 to DOY 309, 2011) reference epoch based IFCBs. From Figure 8, we can see that the 3 d variations of each satellite behave in a similar mode, indicating the feature of sinusoidal variation [14]. In view of the clear orbital periodicity of the IFCB variations as evidenced by Figures 5 and 8, we find a correlation of the variations of IFCB and the included angle between the sun, earth and satellite. The included angle α is illustrated in Figure 9, which has an approximate period of one satellite-rev by definition, because the daily change of the sun elevation above the orbital plane is rather small.

Figure 10 shows the values of included angle for PRN25 and PRN01 for the 3 d cycle. The angle α has a period of 12 h and it shows to be similar in the 3 d.

Figure 11 shows the sinusoidal values of the included angle of PRN25 and PRN01 for 3 d. For comparison, we split the 3 d IFCBs of each satellite into 12 h arcs as shown in Figure 12. Figures 10–12 show clearly the full correlation between the sinusoidal of included angle and 12 h IFCBs.

Based on the data in Figure 11, the approximate expressions for the harmonic coefficients in terms of α have been established for the IFCBs. We model it using the following

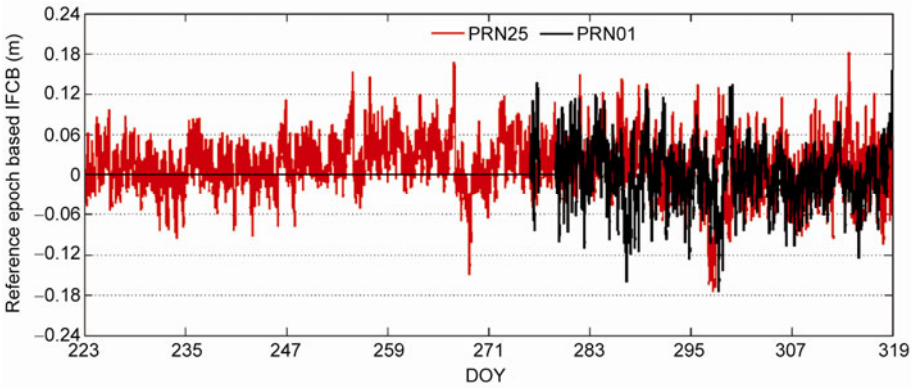

Figure 7 Reference epoch based IFCB of PRN01 and PRN25.

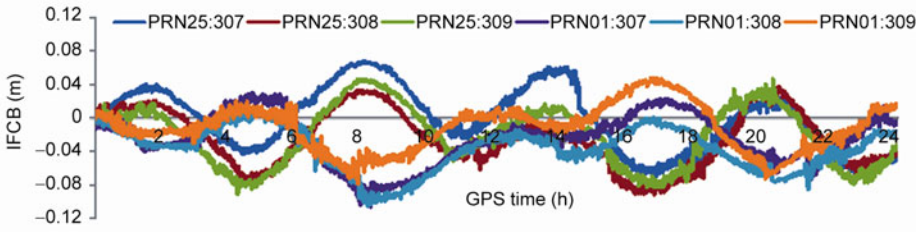

Figure 8 Reference epoch based IFCB of PRN25 and PRN01, DOY 307 to 309.

simple formula constructed by a sinusoidal function of α:

$$\delta = c + \lambda \cdot \sin(\alpha + \theta),\ (\alpha = f(t),\ t = 0 - 24\ \text{h}), \qquad (12)$$

where c is the constant offset reflecting the offset between the sinusoidal function and true IFCBs and θ is phase offset and λ is amplitude. Table 1 presents the fitted coefficients of 3 d for PRN25 and PRN01. In general, θ is quite small, which is due to our assumption that the initial IFCB $\delta(m_0)$ to be 0 and reflects that the variation of IFCBs within the second 12 h of a day repeats the first half cycle of the day. The coefficients c and λ of the 3 d are at the dm level and in general in good agreement for different days up to 4 cm.

Figure 13 shows the comparison of the modeled IFCBs values and true values and presents the standard deviations (STD). In regard to the periodic variations of the IFCBs, the corresponding model matches the actual variation over the 3 d period with a representative accuracy of about 3 cm.

5 Conclusions

We have developed two new approaches for fast IFCB estimation. Using the data of 18 stations spanning 96 d, the apparent IFCBs for the Block IIF satellites PRN25 and PRN01 are investigated. Based on the analysis of the results, the following conclusions can be drawn.

Firstly, although the cycle slip detection in triple-frequency GNSS is studied by some researchers using the DIF phase measurement in simulated data [15], it is important to note that their study neglects the contribution ofthe variational biases to the DIF phase measurement. Numerical results using real triple-frequency data in this paper validates the feasibility of DIF phase measurement in cycle slip detection by comparing the variation of IFCB to

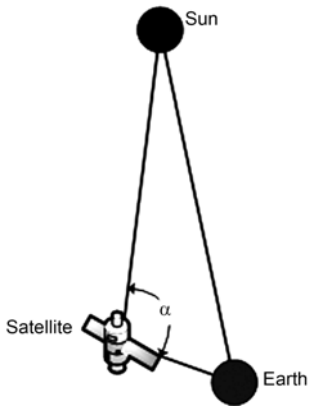

Figure 9 Definition of the included angle α between the sun, earth and satellite.

Table 1 Coefficients of the model

Satellite PRN	Coefficient	DOY307	DOY308	DOY309
01	c (cm)	–9.62	–8.87	–9.96
	λ (cm)	8.93	6.75	10.85
	θ (rad)	–0.22	–0.33	–0.22
25	c (cm)	–9.40	–9.55	–10.60
	λ (cm)	12.26	9.69	11.53
	θ (rad)	–0.09	–0.22	–0.18

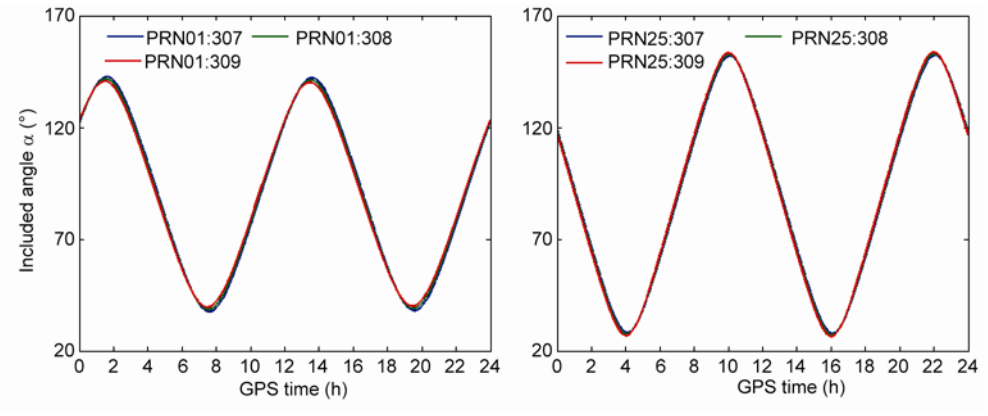

Figure 10 Angle α of PRN01 and PRN25, DOY 307 to 309.

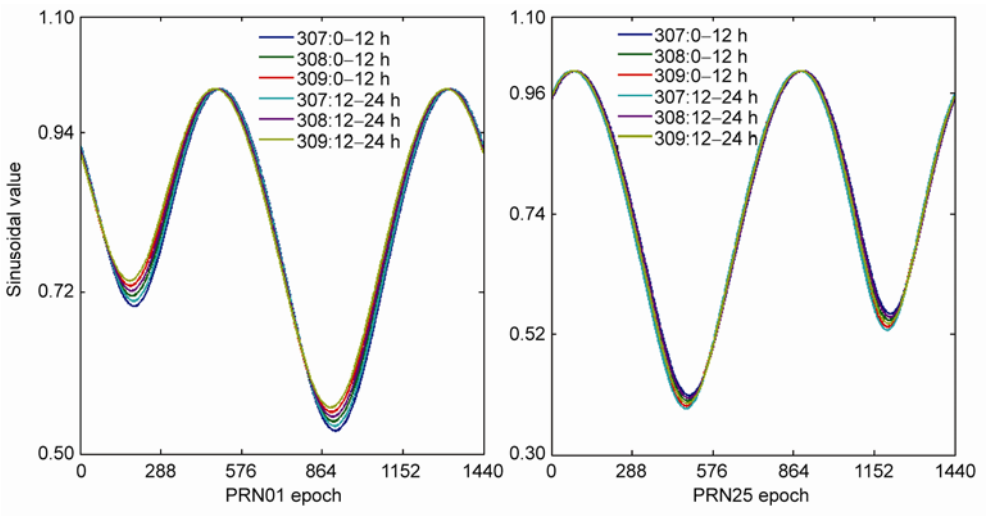

Figure 11 Sinusoidal value of angle α of PRN25, DOY 307 to 309.

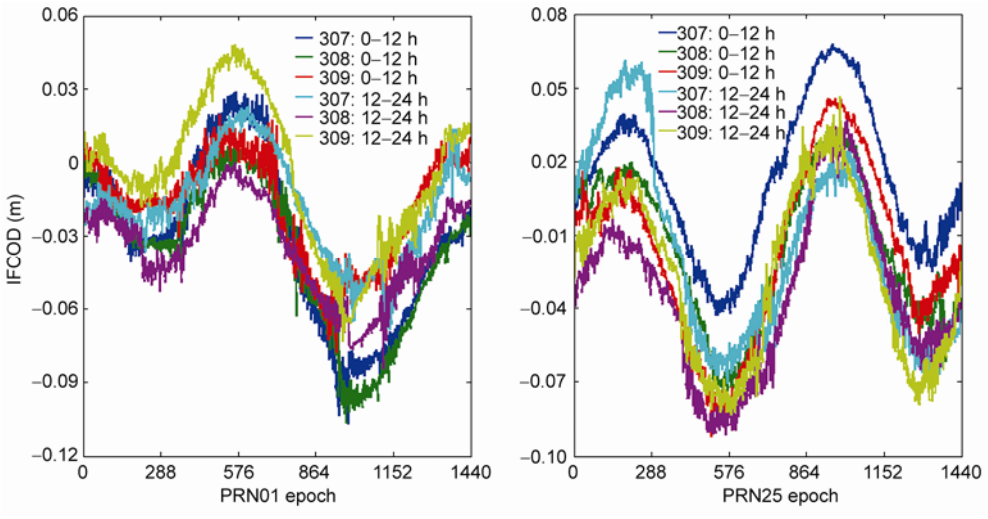

Figure 12 IFCB of PRN01 and PRN25, DOY 307 to 309.

that of DIF phase measurement subject to a slip of one cycle at one frequency.

Secondly, similar to that of PRN25, the PRN01 has also apparent IFCB variations. It is interesting to note that the

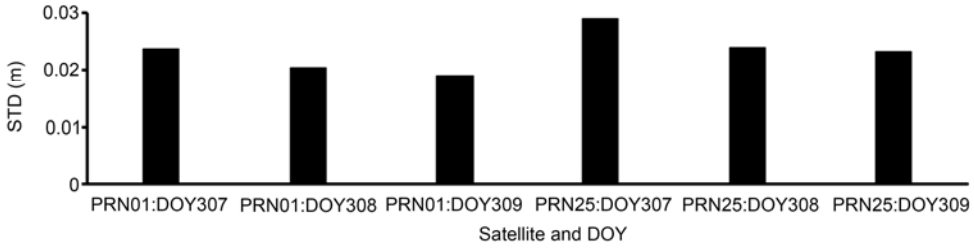

Figure 13 STD of the model compared with the estimated variations of PRN01 and PRN25.

pattern of variation for PRN01 differs to that of PRN25's with a phase shift.

Thirdly, the equality of the SD IFCB derived from two approaches validates the conclusion that the contribution of receiver to the apparent IFCB variations can be neglected, as stated by Montenbruck et al. [8]. The two presented approaches in this paper are more efficient than the traditional absolute clock estimation strategy.

Lastly, the IFCBs of the two Block IIF satellites have notable characterization of periodic variation with a period of 12 h, which is fully correlated with the variation sinusoidal values of the included angle α between the sun, earth and the satellite. A simple and effective model of sinusoidal function of the included angle α is derived. Results show that the accuracy of the model is of 3 cm. Results show also that the IFCBs of the second 12 h of a day repeats cycle of the first half day, and thus the first 12 h IFCBs can be used to model the later 12 h IFCBs with much higher accuracy.

This work was supported by the National Natural Science Foundation of China (Grant Nos. 41204034, 41174023 and 11173049) and the Opening Project of Shanghai Key Laboratory of Space Navigation and Position Techniques (Grant No. Y224 353002).

1 Odijk D. Ionosphere-free phase combinations for modernized GPS. J Survey Eng, 2003, 129(4): 165–173
2 Cocard M, Bourgon S, Kamali O, et al. A systematic investigation of optimal carrier-phase combinations for modernized triple-frequency GPS. J Geod, 2008, 82(9): 555–564
3 Feng Y. GNSS three carrier ambiguity resolution using ionosphere-reduced virtual signal. J Geod, 2008, 82(12): 847–862
4 Feng Y, Li B. Wide area real time kinematic decimetre positioning with multiple carrier GNSS signals. Sci China-Earth Sci, 2010, 53(5): 731–749
5 Li B, Feng Y, Shen Y. Three carrier ambiguity resolution: Distance-independent performance demonstrated using semi-generated triple frequency GPS signals. GPS Solut, 2010, 14: 177–184
6 Kim B, Tinin M. Potentialities of multifrequency ionospheric correction in global navigation satellite systems. J Geod, 2010, 85(3): 159–169
7 Datta-Barua S, Walter T, Blanch J, et al. Bounding higher-order ionosphere errors for the dual-frequency GPS user. Radio Sci, 2008, 43(5): RS5010
8 Montenbruck O, Hugentobler U, Dach R, et al. Apparent clock variations of the Block IIF-1 (SVN62) GPS satellite. GPS Solut, 2011, in press, doi: 10.1007/s10291-011-0232-x
9 Montenbruck O, Hauschild A, Steigenberger P, et al. Three's the challenge: A close look at GPS SVN62 triple-frequency signal combinations finds carrier-phase variations on the new L5. GPS World, 2010, 21(8): 1–8
10 Zumberge J F, Heflin M B, Jefferson D C, et al. Precise point positioning for the efficient and robust analysis of GPS data from large networks. J Geophys Res, 1997, 102(B3): 5005–5017
11 Ge M, Chen J, Dousa J, et al. A computationally efficient approach for estimating high-rate satellite clock corrections in realtime. GPS Solut, 2011, 16: 9–17
12 Li H, Chen J, Wang J, et al. Network based real-time precise point positioning. Adv Space Res, 2010, 46(9): 1218–1224
13 Li H, Wang J, Chen J, et al. The realization and analysis of GNSS network based real-time precise point positioning. Chin J Geophys, 2010, 53(6): 1302–1307
14 Senior K, Ray J, Beard R. Characterization of periodic variations in the GPS satellite clocks. GPS Solut, 2008, 12(3): 211–225
15 Lacy M, Reguzzoni M, Sanso F. Real-time cycle slip detection in triple-frequency GNSS. GPS Solut, 2011, in press, doi: 10.1007/s10291-011-0237-5